QUANTUM SIMULATION

Observing emergent hydrodynamics in a long-range quantum magnet

M. K. Joshi[1], F. Kranzl[1,2], A. Schuckert[3,4], I. Lovas[3,4], C. Maier[1,5], R. Blatt[1,2], M. Knap[3,4]*, C. F. Roos[1,2]*

Identifying universal properties of nonequilibrium quantum states is a major challenge in modern physics. A fascinating prediction is that classical hydrodynamics emerges universally in the evolution of any interacting quantum system. We experimentally probed the quantum dynamics of 51 individually controlled ions, realizing a long-range interacting spin chain. By measuring space-time–resolved correlation functions in an infinite temperature state, we observed a whole family of hydrodynamic universality classes, ranging from normal diffusion to anomalous superdiffusion, that are described by Lévy flights. We extracted the transport coefficients of the hydrodynamic theory, reflecting the microscopic properties of the system. Our observations demonstrate the potential for engineered quantum systems to provide key insights into universal properties of nonequilibrium states of quantum matter.

In quantum many-body systems at equilibrium, the concept of universality asserts that microscopic details do not influence the nature of the emergent quantum phases of matter and their transitions. Rather, symmetries and topology determine the essential macroscopic properties. By contrast, all scales, from low to high energies, are a priori relevant for quantum systems that are driven far from their thermal equilibrium. Recent experimental progress in engineering coherent and interacting quantum systems made it possible to create and explore exotic nonequilibrium states, which can exhibit unconventional relaxation dynamics (*1*–*6*), dynamical phases (*7*–*12*), and transitions between them (*13*, *14*).

Despite this wealth of observed quantum phenomena, a common anticipation is that classical hydrodynamics of a few conserved quantities emerges universally for any complex quantum system, as strong interactions entangle and effectively mix local degrees of freedom (*15*, *16*). However, verifying this assumption, and furthermore determining the nonuniversal transport coefficients of the emergent hydrodynamic theory for specific systems, is challenging. Recently, enormous efforts have been devoted to detect hydrodynamic transport in quantum gases (*17*–*20*) and condensed matter systems (*21*–*24*). Although transport is generally expected to be diffusive, a variety of largely unexplored classes of hydrodynamics have been predicted theoretically, including anomalous subdiffusive (*25*, *26*) and superdiffusive transport (*27*–*29*).

In this work, we experimentally probed the dynamics of a long-range quantum magnet, realized in a quantum simulator of 51 individually controlled ions. We developed a protocol to measure space- and time-resolved spin correlations in an engineered infinite temperature state, enabling us to experimentally establish that hydrodynamics emerges in the nonequilibrium quantum state. By tuning the long-range character of the interactions, we observed a whole family of hydrodynamical universality classes, ranging from normal diffusion to anomalous superdiffusion.

Engineering a long-range quantum magnet

The (pseudo-)spins of our quantum system are realized with two electronic states of the $^{40}Ca^{+}$ ion: $\left|S_{\frac{1}{2}}, m=+\frac{1}{2}\right\rangle$ as $|\downarrow\rangle$ and $\left|D_{5/2}, m=+5/2\right\rangle$ as $|\uparrow\rangle$. The quantum state of individual ions is controlled by a tightly focused, steerable laser beam capable of addressing any ion in the string, in conjunction with a laser beam that collectively interacts with the ions. A two-tone laser field realizes approximately power-law decaying Ising interactions between the (pseudo-)spins by off-resonantly coupling motional and electronic degrees of freedom of the ion chain. Application of a strong transverse field energetically penalizes spin nonconserving contributions (*30*). The effective dynamics are then described by the long-range XY model

$$\hat{H}=\sum_{i<j}\frac{J}{|i-j|^{\alpha}}\left(\hat{\sigma}_i^{+}\hat{\sigma}_j^{-}+\hat{\sigma}_i^{-}\hat{\sigma}_j^{+}\right) \quad (1)$$

where J and α determine the strength and the range of the spin-spin interaction, respectively (*31*). They can be tuned by varying the amplitude and frequency of the two-tone laser field. $\hat{\sigma}_i^{+}$ and $\hat{\sigma}_i^{-}$ are the raising and lowering spin operators acting on the ith spin, respectively. Further experimental details are given in the supplementary materials [(*32*), sections 1 to 4].

Theoretical expectations for late-time dynamics

Conservation laws determine the macroscopic late-time dynamics of quantum systems. In the long-range XY model, the global U(1) symmetry implies the conservation of the total magnetization $\sum_j \hat{\sigma}_j^{z}$. This constrains the relaxation of spin excitations. The long-range couplings enable transport of spin excitations over many lattice sites. As a consequence, at late times the effective dynamics are expected to be governed by classical Lévy flights, which describe random walks with long-distance jumps (Fig. 1A) (*29*, *33*). The probability for a jump of distance ℓ in the Lévy flight is set by the power-law couplings of the long-range XY model as $\sim J^2/\ell^{2\alpha}$ [(*32*), section 8]. These long-distance jumps become irrelevant when the variance of the jump probability is finite. In our model, this is the case for $\alpha > 3/2$, implying conventional diffusion [(*32*), section 8]. However, the variance diverges for $\alpha \leq 3/2$, giving rise to a breakdown of conventional diffusion. The hydrodynamics of our system is therefore expected to be described by the anomalous diffusion equation

$$\partial_t\left\langle\sigma_j^{z}\right\rangle = D_\alpha\nabla^{z_\alpha}\left\langle\sigma_j^{z}\right\rangle \quad (2)$$

where D_α denotes the associated transport coefficient and z_α is the dynamical exponent [(*32*), section 8]. The dynamical exponent z_α relates space and time and hence characterizes transport. For $\alpha > 3/2$, transport is diffusive, and space and time are related by $z_\alpha = 2$. For $1/2 \leq \alpha \leq 3/2$, we predict $z_\alpha = 2\alpha - 1$ (*29*), leading to anomalous superdiffusion. For $\alpha < 1/2$, the spins are so strongly connected that the lattice geometry becomes irrelevant, and a regime with $z_\alpha = 0$ is entered. Therefore, transport is strongly modified by the long-range character of the interactions. The predicted dynamical phase diagram is shown in Fig. 1B.

Experimental signatures of emergent hydrodynamics

Hydrodynamic transport is most directly probed by creating a spin excitation at time $t = 0$ in the center of the chain and tracking how it propagates in space and time, as measured by the unequal-time correlation function

$$C_j(t)=\left\langle\hat{\sigma}_j^{z}(t)\hat{\sigma}_0^{z}\right\rangle_{T=\infty} \quad (3)$$

[1]Institute for Quantum Optics and Quantum Information, Austrian Academy of Sciences, Technikerstraße 21a, 6020 Innsbruck, Austria. [2]Institut für Experimentalphysik, Universität Innsbruck, Technikerstraße 25, 6020 Innsbruck, Austria. [3]Department of Physics and Institute for Advanced Study, Technical University of Munich, 85748 Garching, Germany. [4]Munich Center for Quantum Science and Technology (MCQST), Schellingstraße 4, 80799 München, Germany. [5]AQT, Technikerstraße 17, 6020 Innsbruck, Austria.
*Corresponding author. Email: michael.knap@ph.tum.de (M.K.); christian.roos@uibk.ac.at (C.F.R.)

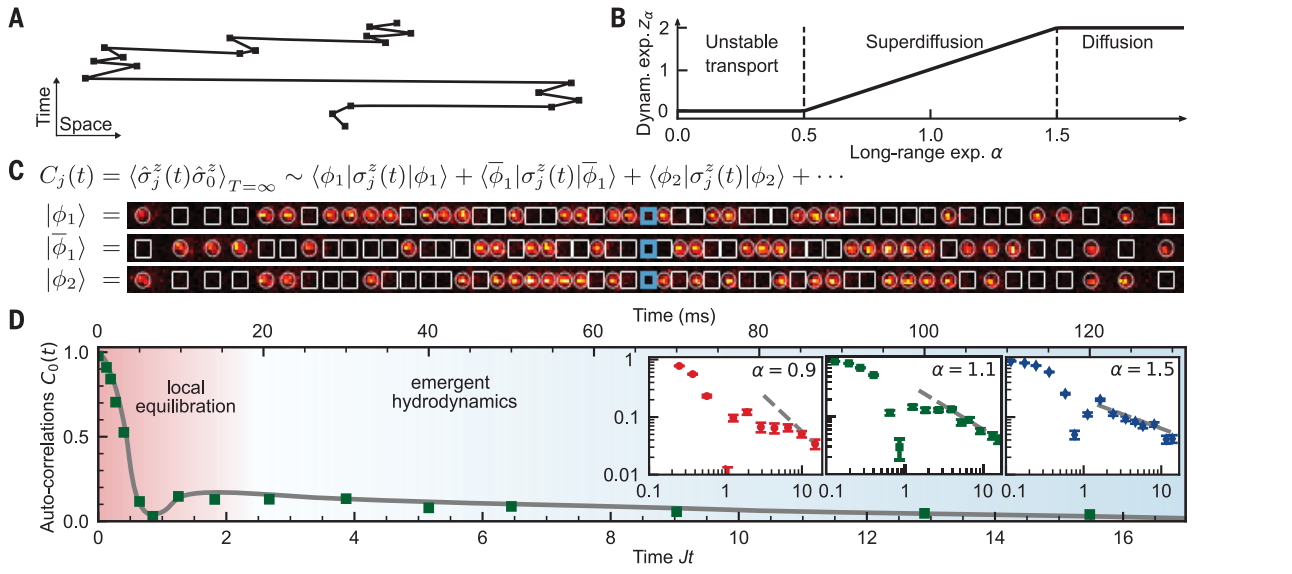

Fig. 1. Emergent hydrodynamics in a long-range quantum magnet. (**A**) In our system, the dynamics of a locally created spin excitation is effectively governed by a hydrodynamic theory of Lévy flights, which are random walks with step sizes drawn from a distribution with algebraic tails. This occasionally leads to long-distance jumps of the excitation. (**B**) The family of hydrodynamic universality classes characterized by a dynamical exponent z_α and a scaling function can be tuned by the power-law exponent α of the spin-spin interactions. (**C**) We measured infinite-temperature correlations by averaging over initial product states and preparing the central ion deterministically in the same state (blue box) [(*32*), section 2]. Picture of three exemplary initial states in a chain of $^{40}Ca^+$ ions ($|\uparrow\rangle$, dark spots; $|\downarrow\rangle$, bright spots). White squares and circles indicate the intended preparation of $|\uparrow\rangle$ and $|\downarrow\rangle$, respectively, achieved with 99% fidelity per ion. (**D**) Measured autocorrelations (green squares) for 51 ions and α = 1.1 (gray line is a guide to the eye). Error bars, denoting the standard error of the mean, are smaller than the symbols [(*32*), section 5]. At short times (red shading), the spin excitation quickly relaxes to a local equilibrium state. At late times (blue shading), global conservation laws constrain the relaxation of spin excitations, leading to a slow power-law decay of the autocorrelations. (Insets) Autocorrelations on a double logarithmic scale for different values of α highlighting the tunable transport. Gray dashed lines are power laws with the predicted exponent from Lévy flights. Here, J = 248, 129, and 116 rad/s for α = 0.9 (51 ions), α = 1.1 (51 ions), and α = 1.5 (25 ions), respectively.

Over the course of the quantum dynamics, the initial excitation has to scatter off a highly excited background to quickly reach the hydrodynamic regime. Therefore, we measured $C_j(t)$ at infinite temperatures T with magnetization ~0.

Measuring spin correlations at different times and preparing an infinite temperature state are both difficult in isolated, engineered quantum systems. We overcame these challenges by expressing the infinite temperature expectation value as an equally weighted trace over product states $|\phi\rangle$ in the $\hat{\sigma}^z$ basis [(*32*), section 10]. When preparing the central spin in the same polarization, we have $\hat{\sigma}_0^z|\phi\rangle = +|\phi\rangle$ (Fig. 1C). The correlation function can then be directly evaluated as $C_j(t) \sim \langle\phi_1|\hat{\sigma}_j z(t)|\phi_1\rangle + \langle\phi_2|\hat{\sigma}_j z(t)|\phi_2\rangle + \ldots$. It can be accurately obtained by sampling a finite number of initial product states [(*32*), section 10]. Yet for a comparatively small and experimentally accessible number of initial states, large statistical fluctuations are expected in the measured correlations. We removed these fluctuations by sampling pairs of conjugate product states, $|\phi\rangle$ and $|\bar{\phi}\rangle$, where in the second configuration all spins are flipped except for the central one. For each pair of product states, initial correlations are unity in the center of the system and zero elsewhere, reproducing directly this property of the full trace (Fig. 1C, first two initial states). With this procedure, convergence is achieved even for a small number of initial product states [(*32*), section 10]. For α = 0.9 and 1.1 and for α = 1.5, respectively, we created 60 and 120 initial product state configurations, each of which was realized, evolved, and measured 50 to 200 times.

The autocorrelation function $C_0(t)$ determines the residual excitation in the center of the chain. We measured $C_0(t)$ for 51 ions (Fig. 1D). The relaxation dynamics occurred in multiple stages. A local equilibrium was reached already after a few collisions, with the abundant excitations of the infinite temperature state. As a consequence, at short times the autocorrelation exhibited a rapidly damped oscillation. At later times, the system entered the hydrodynamic regime and eventually approached a global equilibrium through the slow rearrangement of spin excitations constrained by the conserved magnetization. The longest time to which we could probe transport was limited by the saturation of the correlation function set by the inverse system size. The power-law decay of the correlations became manifest on a double logarithmic scale (Fig. 1D, insets). Our experimental data are consistent with the hydrodynamic theory of Eq. 2, which predicts a power-law exponent of $-1/z_\alpha$ (Fig. 1D, insets, dashed gray lines). Hence, exploiting the experimental control over the long-range exponent α enabled us to tune the transport from normal diffusion to anomalous superdiffusion.

We obtained a more stringent test of the emergent hydrodynamics from the full spatial correlation profile (Fig. 2). We realized the long-range spin model for α = 1.5 with 25 ions (Fig. 2A) and for α = 1.1 with 51 ions (Fig. 2B). At early times (3.1 ms), the quantum dynamics are well-described by an analytic short-time expansion of the equations of motion [(*32*), section 9]. At intermediate times (14.1 ms), the excitation starts spreading through the system, but some quantum coherence remains, indicated by the spatial oscillations. For 25 ions, the measured dynamics compares well with results obtained from exact diagonalization, demonstrating the coherence of our quantum system [(*32*), section 7]. For the 51 ion chain, a comparison to exact diagonalization was not possible because of the exponential growth of the Hilbert space, which reached a dimension of $2^{51} \approx 10^{15}$.

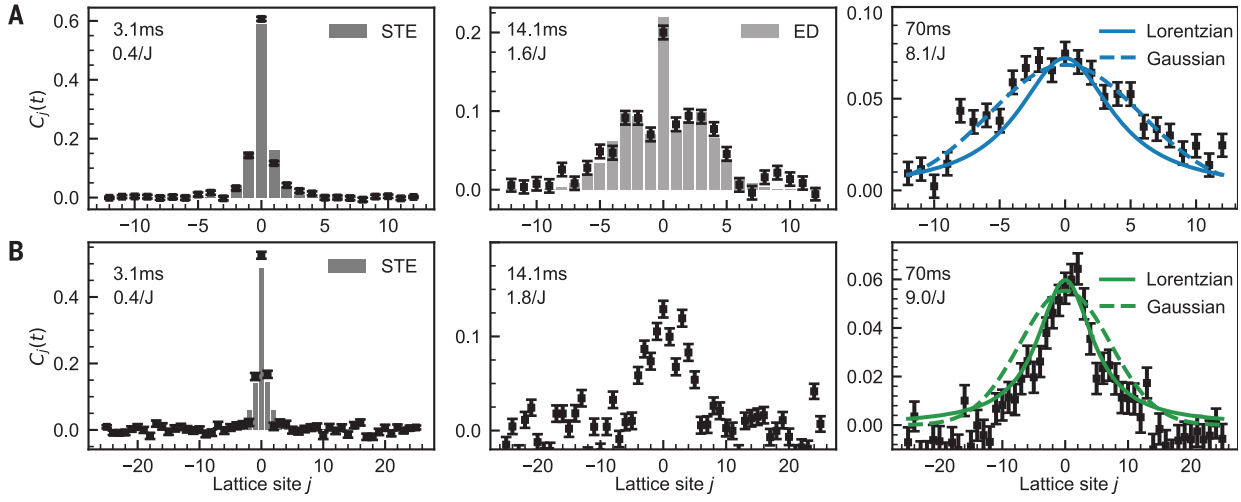

Fig. 2. Spatial correlation profiles. (**A** and **B**) Spatially resolved correlations for (A) $\alpha = 1.5$ for 25 ions and (B) $\alpha = 1.1$ for 51 ions. The spatial correlations are measured at (left) short times, (middle) intermediate times, and (right) in the hydrodynamic late-time regime. STE, analytic short-time expansion; ED, exact diagonalization accessible only for the shorter chain of 25 ions. In the hydrodynamic regime (right), the measured profiles are compared with predictions from Lévy flights. The spatial profile in (A) is compatible with a Gaussian (dashed) and in (B) with a Lorentzian (solid), as supported by the reduced χ^2 values of the fit: (A) $\chi^2_L = 3.9$, $\chi^2_G = 1.3$; (B) $\chi^2_L = 1.4$, $\chi^2_G = 4.8$ (obtained by fitting over the central 27 sites). Here, χ^2_L and χ^2_G are χ^2 values for the Lorentzian and Gaussian fits, respectively.

The quantum dynamics effectively coarsens the system during the time evolution as spatial oscillations with longer wavelengths start to dominate. At the latest times shown (70 ms), interactions have averaged out quantum interference patterns, and the hydrodynamic regime is entered. This became even more apparent in the space-time correlations (Fig. 3A). By contrast, a single excitation on top of a spin-polarized state cannot scatter, and the associated correlations exhibit coherent space-time oscillation patterns instead (Fig. 3B) (*30*).

The theory of Lévy flights predicts the following scaling form for the spatiotemporal profiles

$$C_j(t) = (D_\alpha t)^{-\frac{1}{z_\alpha}} F_\alpha \left[\frac{|j|}{(D_\alpha t)^{1/z_\alpha}} \right] \qquad (4)$$

where F_α is given by the family of stable symmetric distributions (*33*). The scaling between space and time entering the distribution F_α can be deduced directly from the generalized hydrodynamic equation Eq. 2. The distribution F_α cannot be expressed in terms of elementary functions, except for $\alpha = 3/2$, where a Gaussian indicates conventional diffusion, and $\alpha = 1$, where a Lorentzian appears.

The measured hydrodynamic profiles are compatible with a Lorentzian for $\alpha = 1.1$ ($F_{\alpha=1.1}$ is still very close to a Lorentzian) and with a Gaussian for $\alpha = 1.5$ (χ^2 analysis is provided in Fig. 2, right), which is in agreement with Eq. 4.

Determining scaling exponents and coefficients

Close to equilibrium phase transitions, correlation functions show self-similarity as a function of the distance to the critical point and can be characterized by a set of universal scaling exponents as well as scaling functions (*34*). Hydrodynamics predicts a self-similar scaling of correlations as a function of time, characterized by the dynamical scaling exponent z_α and the scaling function F_α (*35*). Whereas z_α and F_α solely depend on the asymptotic decay of the interactions and can be predicted from purely hydrodynamic reasoning, the transport coefficient D_α is not universal and depends on the full quantum many-body spectrum. It is therefore challenging to make predictions of D_α by using analytical or numerical methods. To verify Eq. 4, we rescaled $C_j(t)$ and space j as shown in Fig. 4, leading to a scaling collapse. By fitting the stable symmetric distributions to the collapsed data, we obtained a transport coefficient of $D_\alpha/J = 0.5^{+0.2}_{-0.1}$, $0.8^{+0.3}_{-0.2}$, and $2.6^{+0.9}_{-0.7}$ for $\alpha = 0.9$, 1.1, and 1.5, respectively [(*32*), section 6]. From exact diagonalization, we obtained $D_\alpha/J = 1.9^{+0.7}_{-0.5}$ for $\alpha = 1.5$.

Discussion

Large, coherent quantum systems with local control provide key insights into fundamental properties of nonequilibrium quantum states. In our experiment, we measured the emergent macroscopic hydrodynamics in an infinite temperature state of a strongly interacting spin chain—a regime that is notoriously challenging to describe by controlled analytical or numerical calculations. By measuring the full spatiotemporal profile of the hydrodynamic scaling functions, we experimentally established a tunable family of transport that ranges from conventional diffusion to anomalous superdiffusion.

One prospect is to investigate the generality of the dynamical phase diagram (Fig. 1B) for other models with long-range interactions that conserve the total magnetization or charge. An example could be the long-range Heisenberg model, which can be realized in our system with suitably designed Floquet protocols (*36*). Moreover, our tools for measuring high-temperature correlations can be readily applied to other quantum devices with local control, including quantum gas microscopes, Rydberg atom arrays, and superconducting qubits. Diffusion constants measured in controlled synthetic quantum matter could serve as a benchmark for newly developed numerical methods and for comparing different experimental platforms that realize the same model. Creating finite temperature states in the vicinity of a thermal phase transition with synthetic quantum matter would enable the study of emergent dynamic critical phenomena, describing a modified hydrodynamics in which additional conservation laws are introduced by the order parameter (*37*). Emergent hydrodynamics could also be tested for different initial states, such as certain product states (*15*).

Note added in proof: During the completion of this manuscript, we became aware of related work demonstrating superdiffusive transport in an integrable Heisenberg chain with nearest-neighbor superexchange interactions (*38*).

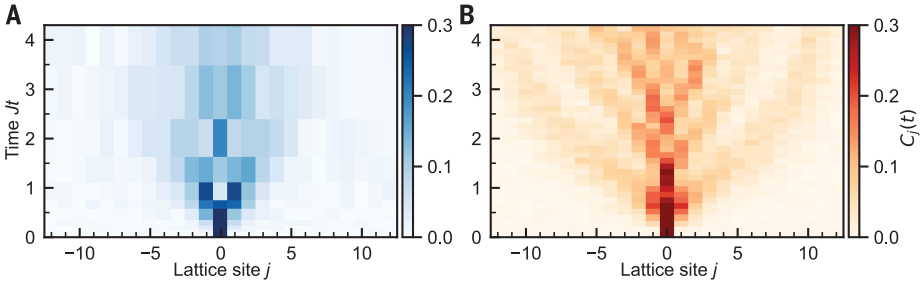

Fig. 3. Contrasting the infinite temperature background with the spin polarized background. (**A**) The deterministically prepared excitation of the central ion strongly interacts with all the other excitations of the infinite temperature background and slowly spreads through the system following the laws of classical hydrodynamics. (**B**) By contrast, a single excitation on top of the fully down-polarized state ↓ ... ↓↑↓ ...↓ has no other excitations to scatter off and therefore spreads freely, exhibiting quantum interference patterns. Data are measured for 25 ions with power-law exponent α = 1.5.

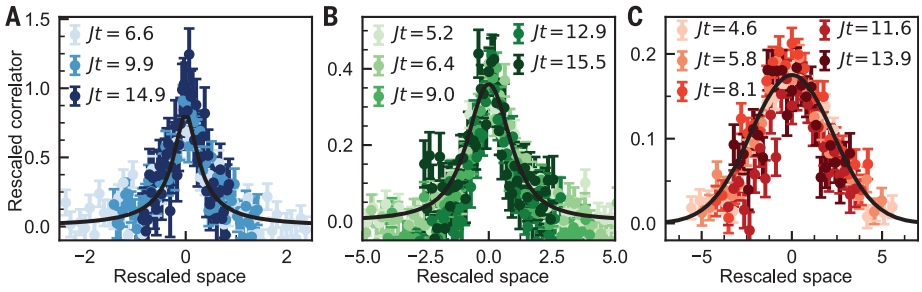

Fig. 4. Extracting transport coefficients. At late times, the correlations exhibit a self-similar scaling, relating space and time with a microscopic transport coefficient D_α. Shown are rescaled correlations $\tau_x C_j(t)$ as a function of rescaled space j/τ_x, where $\tau_x = (Jt)^{1/z_\alpha}$. (**A**) α = 0.9, 51 ions. (**B**) α = 1.1, 51 ions. (**C**) α = 1.5, 25 ions. Correlations are shown for times $Jt > 5$; darker colors correspond to later times.

REFERENCES AND NOTES

1. M. Gring *et al.*, *Science* **337**, 1318–1322 (2012).
2. J. G. Bohnet *et al.*, *Science* **352**, 1297–1301 (2016).
3. Y. Tang *et al.*, *Phys. Rev. X* **8**, 021030 (2018).
4. H. Bernien *et al.*, *Nature* **551**, 579–584 (2017).
5. E. Guardado-Sanchez *et al.*, *Phys. Rev. X* **10**, 011042 (2020).
6. S. Scherg *et al.*, *Nat. Commun.* **12**, 4490 (2021).
7. M. Schreiber *et al.*, *Science* **349**, 842–845 (2015).
8. J. Smith *et al.*, *Nat. Phys.* **12**, 907–911 (2016).
9. A. M. Kaufman *et al.*, *Science* **353**, 794–800 (2016).
10. T. Brydges *et al.*, *Science* **364**, 260–263 (2019).
11. M. Prüfer *et al.*, *Nature* **563**, 217–220 (2018).
12. S. Erne, R. Bücker, T. Gasenzer, J. Berges, J. Schmiedmayer, *Nature* **563**, 225–229 (2018).
13. P. Jurcevic *et al.*, *Phys. Rev. Lett.* **119**, 080501 (2017).
14. J. Zhang *et al.*, *Nature* **551**, 601–604 (2017).
15. J. Lux, J. Müller, A. Mitra, A. Rosch, *Phys. Rev. A* **89**, 053608 (2014).
16. A. Bohrdt, C. B. Mendl, M. Endres, M. Knap, *New J. Phys.* **19**, 063001 (2017).
17. C. Cao *et al.*, *Science* **331**, 58–61 (2011).
18. A. Sommer, M. Ku, G. Roati, M. W. Zwierlein, *Nature* **472**, 201–204 (2011).
19. U. Schneider *et al.*, *Nat. Phys.* **8**, 213–218 (2012).
20. P. T. Brown *et al.*, *Science* **363**, 379–382 (2019).
21. D. A. Bandurin *et al.*, *Science* **351**, 1055–1058 (2016).
22. J. Crossno *et al.*, *Science* **351**, 1058–1061 (2016).
23. P. J. W. Moll, P. Kushwaha, N. Nandi, B. Schmidt, A. P. Mackenzie, *Science* **351**, 1061–1064 (2016).
24. C. Zu *et al.*, *Nature* **597**, 45–50 (2021).
25. A. Gromov, A. Lucas, R. M. Nandkishore, *Phys. Rev. Res.* **2**, 033124 (2020).
26. J. Feldmeier, P. Sala, G. De Tomasi, F. Pollmann, M. Knap, *Phys. Rev. Lett.* **125**, 245303 (2020).
27. M. Ljubotina, M. Žnidarič, T. Prosen, *Nat. Commun.* **8**, 16117 (2017).
28. V. B. Bulchandani, S. Gopalakrishnan, E. Ilievski, *J. Stat. Mech.* **2021**, 084001 (2021).
29. A. Schuckert, I. Lovas, M. Knap, *Phys. Rev. B* **101**, 020416 (2020).
30. P. Jurcevic *et al.*, *Nature* **511**, 202–205 (2014).
31. C. Monroe *et al.*, *Rev. Mod. Phys.* **93**, 025001 (2021).
32. Materials and methods are available as supplementary materials.
33. V. Zaburdaev, S. Denisov, J. Klafter, *Rev. Mod. Phys.* **87**, 483–530 (2015).
34. J. Cardy, *Scaling and Renormalization in Statistical Physics* (Cambridge Univ. Press, 1996).
35. D. Forster, *Hydrodynamic Fluctuations, Broken Symmetry, and Correlation Functions* (CRC Press, 1975).
36. S. Birnkammer, A. Bohrdt, F. Grusdt, M. Knap, arXiv:2012.09185 [cond-mat.quant-gas] (2020).
37. P. C. Hohenberg, B. I. Halperin,*Rev. Mod. Phys.* **49**, 435–479 (1977).
38. D. Wei *et al.*, *Science* **376**, 716–720 (2022).
39. M. K. Joshi *et al.*, Observing emergent hydrodynamics in a long-range quantum magnet, Zenodo (2022); https://doi.org/10.5281/zenodo.6256977.

ACKNOWLEDGMENTS

Funding: We acknowledge support from the Technical University of Munich–Institute for Advanced Study, funded by the German Excellence Initiative and the European Union FP7 under grant agreement 291763; the Max Planck Gesellschaft (MPG) through the International Max Planck Research School for Quantum Science and Technology (IMPRS-QST); the Deutsche Forschungsgemeinschaft (DFG; German Research Foundation) under Germany's Excellence Strategy–EXC–2111–390814868; as well as the Munich Quantum Valley, which is supported by the Bavarian state government with funds from the Hightech Agenda Bayern Plus. The project leading to this application has received funding from the European Union's Horizon 2020 research and innovation programme under grant agreement no. 817482, from the European Research Council (ERC) under the European Union's Horizon 2020 research and innovation programme (grant agreement no. 851161, no. 741541, and no. 771537), the Institut für Quanteninformation GmbH, and the Austrian Science Fund through the SFB BeyondC (F7110). **Author contributions:** M.K.J., C.M., M.K., and C.F.R. devised the research. A.S., I.L., and M.K. developed the theoretical protocols. M.K.J., F.K., C.M., R.B., and C.F.R. contributed to the experimental setup. M.K.J. and F.K. performed the experiments. M.K.J., A.S., I.L., M.K., and C.F.R. analyzed the data, and M.K.J., A.S., and C.F.R. carried out numerical simulations. M.K.J., A.S., M.K., and C.F.R. wrote the manuscript. All authors contributed to the discussion of the results and the manuscript. **Competing interests:** The authors declare no competing interests. **Data and materials availability:** All data analysis and simulation codes along with the experimental data are available on Zenodo (*39*).

SUPPLEMENTARY MATERIALS

science.org/doi/10.1126/science.abk2400
Materials and Methods
Supplementary Text
Figs. S1 to S9
References (*40*–*46*)

Submitted 30 June 2021; accepted 10 March 2022
10.1126/science.abk2400